

AN ESTIMATE OF THE DETECTABILITY OF RISING FLUX TUBES

A. C. BIRCH¹, D. C. BRAUN¹, AND Y. FAN²

¹ NWRA, CoRA Division, 3380 Mitchell Lane, Boulder, CO 80301, USA; aaronb@cora.nwra.com

² High Altitude Observatory, National Center for Atmospheric Research, P.O. Box 3000, Boulder, CO 80307, USA

Received 2010 June 11; accepted 2010 August 30; published 2010 October 18

ABSTRACT

The physics of the formation of magnetic active regions (ARs) is one of the most important problems in solar physics. One main class of theories suggests that ARs are the result of magnetic flux that rises from the tachocline. Time–distance helioseismology, which is based on measurements of wave propagation, promises to allow the study of the subsurface behavior of this magnetic flux. Here, we use a model for a buoyant magnetic flux concentration together with the ray approximation to show that the dominant effect on the wave propagation is expected to be from the roughly 100 m s^{-1} retrograde flow associated with the rising flux. Using a B-spline-based method for carrying out inversions of wave travel times for flows in spherical geometry, we show that at 3 days before emergence the detection of this retrograde flow at a depth of 30 Mm should be possible with a signal-to-noise level of about 8 with a sample of 150 emerging ARs.

Key words: Sun: dynamo – Sun: helioseismology – Sun: interior – Sun: oscillations

1. INTRODUCTION

The physical mechanism behind the formation of magnetic active regions (ARs) is one of the central problems in solar physics. Magnetic flux rising from the tachocline is one possible cause of ARs (e.g., Fan 2009). Local helioseismology (see, e.g., Gizon & Birch 2005 for a review) can, in principle, be used to detect and study magnetic flux rising through the convection zone.

It is not yet feasible to construct a complete three-dimensional (3D) MHD model of rising AR flux tubes, extending from the base of the solar convection zone up into the visible solar atmosphere. Recent 3D simulations of buoyantly rising flux tubes in a rotating spherical shell representing the solar convective envelope (Fan 2008; Jouve & Brun 2009) cover depths from the base of the solar convection zone to about 20 Mm below the surface. Because of the rapid decrease of the pressure scale height in the top layers of the solar convection zone which demands increasing numerical resolution, it is not yet feasible to extend such global scale 3D models all the way to the photosphere. Furthermore, there is an increased complexity in the thermodynamics of the plasma in the top layer of the solar convection zone due to ionization effects and radiative energy transport (see review by Nordlund et al. 2009).

There have been a number of helioseismic searches for rising flux tubes (see Kosovichev 2009 for a recent review). Chang et al. (1999) used acoustic imaging (Chang et al. 1997) to suggest an increase in wave speed at depths from the surface down to 40 Mm (the largest depth that was studied) associated with the emergence of AR NOAA 7978, though cautioned that a large part of the apparent signal may be a result of surface effects (e.g., the effect of photospheric magnetic fields on wave propagation). Kosovichev et al. (2000) used time–distance helioseismology (Duvall et al. 1993) to search for changes in wave speed associated with the emergence of an AR which emerged in 1998 January. This study found changes in subsurface wave speed at the time of emergence. Similar results were obtained by Jensen et al. (2001) for an emerging AR on 1998 January 11–12. In another case study, Zharkov & Thompson (2008) concluded

that there was little change in the subsurface wave speed that preceded the emergence of NOAA 10790. Komm et al. (2009) used the ring diagram method (Hill 1988) and found that, for a sample of about 800 ARs, increasing upward velocity at depths greater than about 10 Mm and less than 16 Mm is associated with emerging flux regions, with the upward velocity increasing by a fraction of a m s^{-1} over a period of roughly 5 days.

Here, we will employ the ray approximation (e.g., Kosovichev & Duvall 1997) to show that the rising flux models of Fan (2008) imply wave travel-time shifts of approximately 1 s. The dominant cause of these travel-time shifts is the strong (of order 100 m s^{-1}) retrograde flow associated with the rising flux. We develop a method for inversions in spherical geometry for the flows associated with these rising flux tubes. We use this inversion method, together with the noise estimates of Braun & Birch (2008), to estimate the signal-to-noise ratios that would be expected for a search for rising flux tubes using time–distance helioseismology. We conclude that a sample of time–distance measurements for about 150 rising flux tubes is sufficient to detect the flows associated with these tubes with a signal-to-noise ratio of about 8 at a depth of 30 Mm about 3 days before emergence, and with a signal-to-noise ratio of about 4 at 5 days before emergence.

2. MODELS OF RISING FLUX TUBES

The model of a rising flux tube used in this study is the simulation labeled “LNT” (standing for Low Negative Twist) in Fan (2008). The details of the numerical model are described in Fan (2008). Briefly, we solve a set of anelastic MHD equations in a rotating (with a solar-like rate of $2.7 \times 10^{-6} \text{ rad s}^{-1}$) spherical-shell domain of $r \in [r_c, r_t]$, where r is distance from the center of the Sun, $r_c = 0.722 R_\odot$ is the base of the convection zone, and $r_t = 0.977 R_\odot$ is at about 16 Mm below the photosphere, $\theta \in [0, \pi/2]$ and $\phi \in [0, \pi/2]$, where θ is the co-latitude and ϕ is the longitude. The boundary conditions are periodic in the ϕ direction and are non-penetrating, stress-free, electrically conducting walls for the bottom and top boundaries and the θ boundaries. The domain is resolved by a grid with (256, 512, 512) grid points in (r, θ, ϕ) . Turbulent convective flows

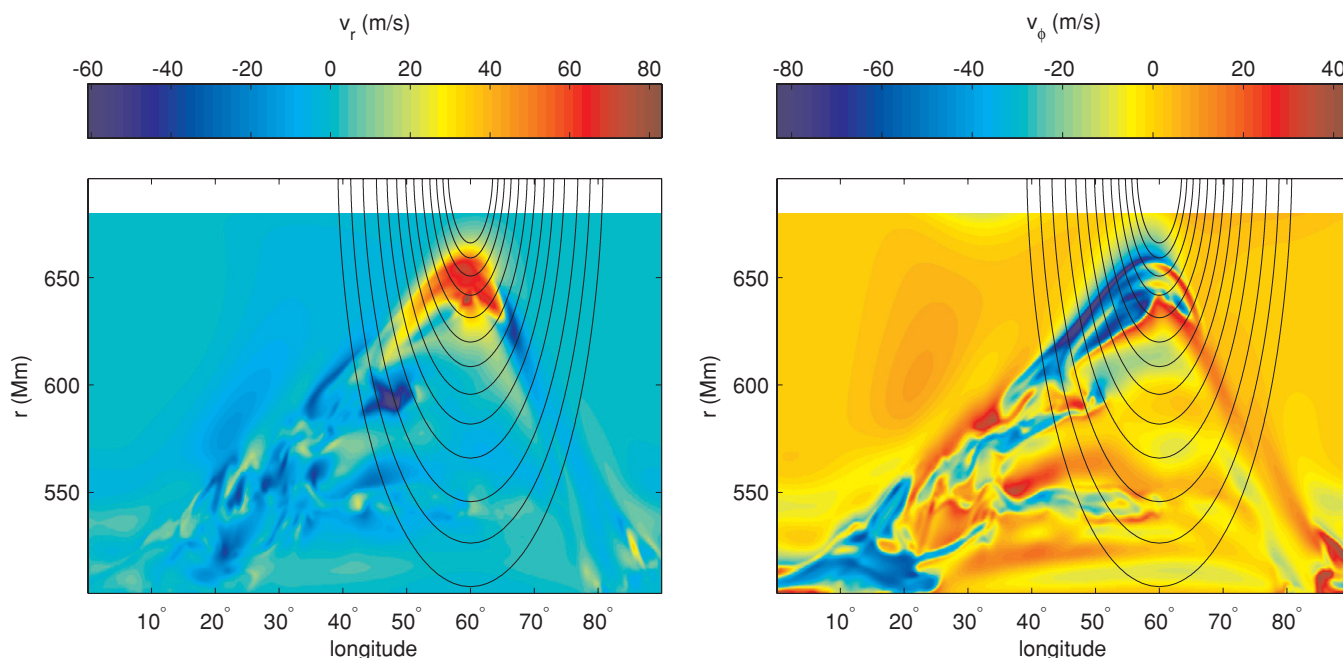


Figure 1. Slices at the latitude of $17^{\circ}8$ through the radial (left panel) and azimuthal (right panel) components of the flow field associated with the rising flux tube model LNT of Fan (2008) at about 5 days before emergence. The curved black lines show ray paths corresponding to the 13 distances used in the inversions shown in this Letter. The flows have amplitudes of up to about 80 m s^{-1} . The retrograde flow near the apex of the rising flux tube is due to the Coriolis force as the flux tube is moving away from the rotation axis of the Sun. The simulation domain extends upward to within about 16 Mm of the photosphere.

are ignored by assuming an adiabatically stratified background fluid. Initially a twisted toroidal flux tube with a radius of about 0.1 times the local pressure scale height is placed just slightly above the base of the model convective envelope, at an initial latitude of 15° . The initial magnetic flux in the tube is about 10^{23} Mx and about half of this flux is expected to rise in a cohesive form to the photosphere (Fan 2008). An initial temperature variation along the tube is imposed such that the mid cross-section of the toroidal tube is in approximate thermal equilibrium with the surroundings and is most buoyant: the buoyancy declines with increasing azimuthal distance from the mid cross-section and tends to approximate neutral buoyancy at the two ends. Subsequently, the toroidal flux tube rises under its buoyancy, and an Ω -shaped asymmetric emerging tube develops. The velocity field for the Ω -shaped tube is shown in Figure 1.

3. THE DETECTABILITY OF RISING FLUX TUBES

In order to estimate the detectability of the rising flux tube described in Section 2, we have developed a simple spherical 3D ray-approximation-based inversion method for estimating the flow field in the solar interior given a set of measurements of travel-time differences (see the Appendix for details). The inversion employs a separable B-spline (de Boor 2001) expansion of the flow field (Equation (A1)) and is carried out using a regularized least squares inversion (e.g., Kosovichev 1996, in the context of time–distance helioseismology) with a regularization term based on the total integral of the square of the amplitude of the flow (Equation (A3)). An advantage of using B-splines is that they provide easily customizable and spatially variable spatial resolution. In the present case, the spline functions are chosen such that the spatial resolution is best nearest the flux tube.

The ray approximation (Kosovichev & Duvall 1997) provides estimates of the wave travel-time shifts that result from the

change in the wave speed associated with the rising flux tube. In the model of Section 2, the fractional wave-speed perturbations due to temperature fluctuations are of order 2×10^{-6} and those due to the magnetic field are of order 10^{-5} . Compared with $\|\mathbf{v}\|/c \approx 10^{-3}$, where \mathbf{v} is the fluid velocity and c is the sound speed, these effects are negligible. Thus, for the models of Section 2, the travel-time shifts caused by flows dominate, by several orders of magnitude, over the travel-time shifts caused by changes in structure or by the magnetic fields. As a result, in this Letter we will only consider inversions for velocity.

The ray approximation is expected to be valid when the wavelength of the waves is small compared to the length scale of the velocity field. The horizontal wavelength of a wave with a lower turning point at a depth of 60 Mm below the photosphere and a period of 5 minutes is about three heliocentric degrees. This is similar to the smallest length scales in the flow field (see Figure 1) and is smaller than the largest length scales. As a result, we expect the ray approximation to be reasonable. In the time intervals we will consider (24 hr), the velocity field associated with the rising flux moves upward through approximately 1/3 of its vertical thickness. Thus, we approximate the flux tube as steady when applying the ray approximation.

The flow in the rising flux tube is dominantly in the ϕ and r directions; as a result we choose to use only deep focusing, quadrant averaged, east–west travel-time differences. In this geometry, the measurement is of the difference in travel times for eastward and westward traveling waves (see, e.g., Braun & Birch 2008 for a discussion of this measurement geometry). Here, we model measurements that are made from tracked data to account for solar rotation (e.g., Braun & Birch 2008). We will use Δ to denote the distance between the quadrants. The point midway between the two quadrants will be referred to as the “measurement” or “center” point, this is the horizontal location at which the ray path reaches its maximum depth. Figure 2 shows the center locations of the travel-time difference measurements for $\Delta = 10^{\circ}8$ for the example inversions shown

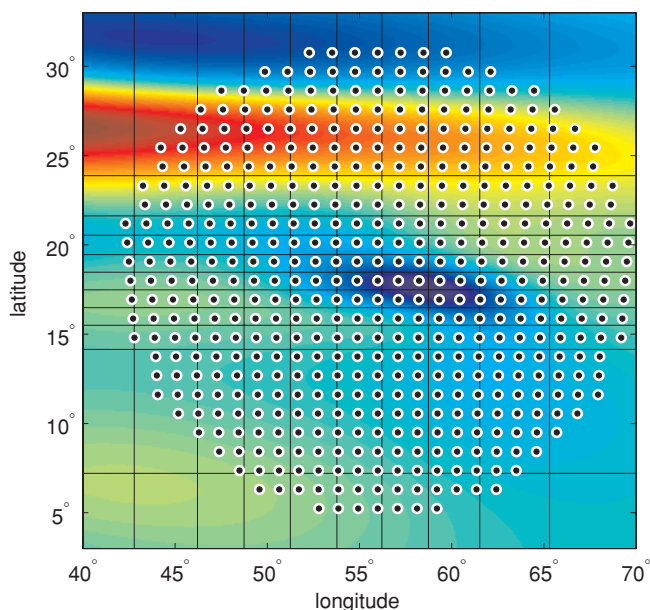


Figure 2. Measurement points (black circles) for the case $\Delta = 10^{\circ}8$ and a slice through the ϕ component of the flow at about 30 Mm below the photosphere (colors, with blue indicating retrograde flows and red showing prograde flows, see Figure 1). The grid of measurement points was selected such that the closest distance between measurement points is roughly half of the dominant wavelength of the waves contributing to the measurements at this distance. As a result, we expect that the realization noise in the measurements will be approximately uncorrelated. The black lines of constant longitude (latitude) show the positions of the maxima of the $B^{(\phi)}$ ($B^{(\theta)}$) spline functions used in the expansion of the flow. The blue retrograde feature at latitude of about 18° and longitude 58° is the flow associated with the rising flux. The large-scale prograde flow at higher latitude is part of the surrounding flow induced by the rise of the flux tube. It is probably caused by the Coriolis force acting on a poleward and downward flow away from the main upwelling flow of the rising flux tube.

later in this Letter. We have chosen to use center points that are separated by about one half of the dominant wavelength that is selected by the measurement filters. In this case, the travel-time measurements are expected to be essentially uncorrelated (e.g., Gizon & Birch 2004). As a result, in the inversion we have assumed uncorrelated input measurements (the generalization to including an arbitrary covariance matrix was shown by Couvidat et al. 2005). In the inversions shown here we have used 13 different distances (from about 7° to about 40°) and a grand total of 5843 measurement points.

The inversion requires estimates of the noise level in each measurement. Braun & Birch (2008) used Michelson Doppler imager data (Scherrer et al. 1995) to estimate that the noise in a single east–west travel-time difference, using 1 day of averaging, is about 4 s and is essentially independent of depth over the range of depths explored in that paper (and which we employ in the current work). This estimate includes realization noise as well as the noise from convective flows. For the remainder of this Letter, we will adopt this noise estimate. Here, we consider inversions in which the noise level is set to $\sigma = 4/\sqrt{150} \text{ s} \approx 0.33 \text{ s}$. This is what would be expected for the case of an average over 150 examples of rising flux tubes, measured for 1 day each. A sample of 150 ARs that emerge on the visible disk can be found in less than one solar cycle. For example, Kosovichev & Stenflo (2008) found a sample of 715 emerging ARs with fluxes between about 10^{21} and 10^{22} Mx that emerged within 30° of the central meridian between 1996 and 2008. Based on previous results from thin flux tube simulations,

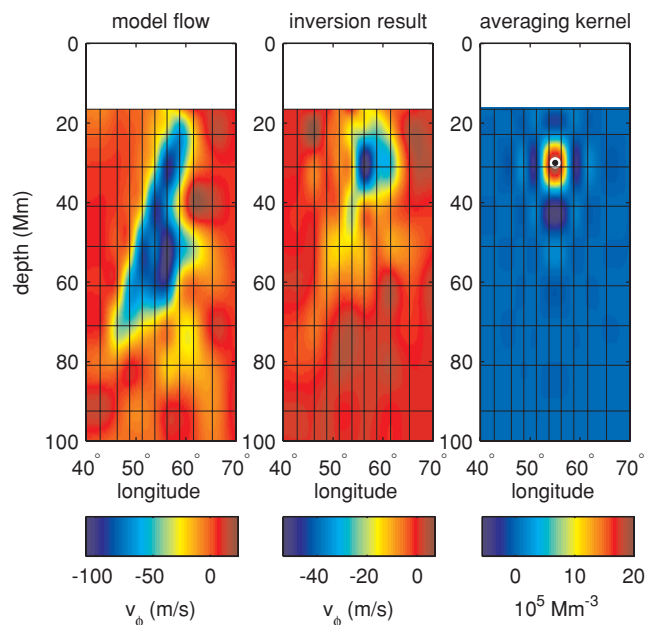


Figure 3. Model flow, example inversion result, and an example averaging kernel at about 3 days before emergence. The left panel shows a slice at latitude $17^{\circ}8$ of the B-spline representation (Equation (A1)) of the ϕ component of the flow from the model. The middle panel shows a slice, at the same latitude, through an example inversion result for a particular choice of the regularization parameter ($\lambda = 2 \times 10^{-6} \text{ Mm}^{-3} (\text{m s}^{-1})^{-2}$, see Equation (A3)). The right most panel shows a slice through the averaging kernel for the inversion at a depth of 40 Mm and longitude of 55° . In all panels the horizontal lines show the maxima of the functions $B^{(r)}(r)$ and the vertical lines show the maxima of the $B^{(\phi)}(\phi)$.

the magnitude of the retrograde flow associated with the rising flux is not expected to depend strongly on the total magnetic flux in this regime (Fan 2009).

In the remainder of this section, we will study the signal-to-noise ratios that could be expected for inversions for the flow fields associated with the model for a rising flux tube of Section 2. The general procedure is as follows: (1) use the known flow field together with the ray approximation to compute a set of noise-free travel-time differences, (2) add Gaussian noise (with the amplitude discussed above) to the travel-time differences, and (3) carry out inversions of these synthetic data. In order to compute signal-to-noise ratios, we estimate the signal by computing the average over many inversions and estimate the noise level by a formal propagation of the noise estimates through the inversion procedure.

Figure 3 shows an example inversion result for a particular choice of regularization parameter λ (Equation (A3)) for the flux tube at 3 days before emergence. For this λ , the noise level is about 5 m s^{-1} at a depth 30 Mm and the inferred flow has an amplitude of about 40 m s^{-1} . Thus, the signal-to-noise ratio for the detection of the flux tube is about 8. This ratio can also be simply estimated. The travel-time difference due to a flow of $v = 40 \text{ m s}^{-1}$ at a depth of 30 Mm (the sound speed at this depth is $c \approx 70 \text{ km s}^{-1}$) for a travel distance of 100 Mm (this gives a lower turning point depth of about 30 Mm) is about 1 s. The noise level in a single measurement is 0.33 s and of order 10 rays are sensitive to the flow within the resolution of the inversion. Thus, we expect the signal-to-noise ratio to be approximately $\sqrt{10}(1 \text{ s})/(0.33 \text{ s}) \approx 10$ (this estimate depends on the inversion weights largely having the same sign, which is the case for the current choice of regularization parameter). For

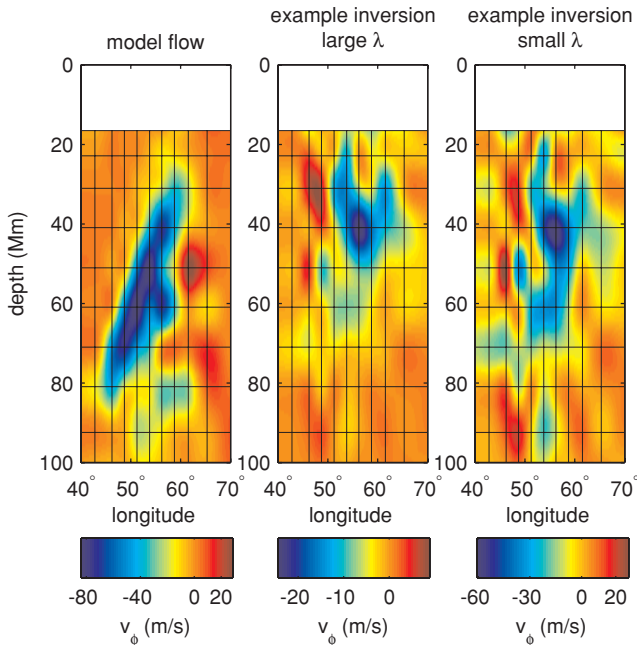


Figure 4. Model flow and two example inversion results at about 5 days before emergence. The left panel shows a slice at latitude $17^{\circ}8'$ of the B-spline representation (Equation (A1)) of the ϕ component of the flow from the model. The middle and right panels show slices through example inversion results for two different values of the regularization parameter ($\lambda = 2 \times 10^{-6} \text{ Mm}^{-3} (\text{m s}^{-1})^{-2}$ in the middle panel and $\lambda = 2.5 \times 10^{-7} \text{ Mm}^{-3} (\text{m s}^{-1})^{-2}$ in the right panel).

the case of smaller regularization parameters, the noise level of the inversion increases. From the results of this example calculation, we expect that a sample of about 150 rising flux tubes should be sufficient to test the model of Fan (2008) at about 3 days before emergence.

The right-hand panel of Figure 3 shows a slice through the averaging kernel for the inversion result at a depth of 40 Mm, latitude $17^{\circ}8'$, and longitude of 55° . For this choice of regularization parameter, there are negative side lobes on the averaging kernel. The spatial extent of the averaging kernel is very similar to the size of the feature seen in the inversion; the inversion is not resolving any of the structure of the flow field.

Figure 4 shows two example inversions for the case of the rising flux tube model at 5 days before emergence. For the larger regularization parameter ($\lambda = 2 \times 10^{-6} \text{ Mm}^{-3} (\text{m s}^{-1})^{-2}$) the inversion is able to qualitatively detect the retrograde velocity of the tube to a depth of about 40 Mm. For the smaller regularization parameter ($\lambda = 2.5 \times 10^{-7} \text{ Mm}^{-3} (\text{m s}^{-1})^{-2}$), the flow can be seen down to roughly 60 Mm, but at the cost of many artifacts due to noise. For the case of the larger regularization parameter, the signal-to-noise ratio at a depth of 40 Mm is about 4.

4. DISCUSSION

We used the ray approximation to compute the travel-time differences that would be expected in the rising flux tube model LNT of Fan (2008). We find that the travel-time differences are of order 1 s and are due largely to strong retrograde flows. The travel-time shifts due to changes in the local sound speed and the direct effect of the magnetic field on the wave speed are several orders of magnitude smaller.

In the inversion presented here we have only used one-skip travel-time measurements. It is an open question if the signal-

to-noise ratio of the inversion could be significantly improved by using measurements of multiple-skip travel times.

Several effects may significantly alter the results of the rising flux tube model. Convective flows may further distort the rising flux tube and its associated flow patterns. The effect of the strong radial shear in the top layers (depth of about 20 Mm) of the solar convection zone is not included. The numerical diffusion intrinsic to the 3D numerical model weakens the flux tube field strength and reduces the amplitude of the flow patterns (for both the rise speed and the retrograde flow speed). Improved 3D models of rising flux tubes that incorporate turbulent convection and mean flows in the solar convection zone and also with a reduced numerical diffusion are needed to improve our estimate of the likely helioseismic signatures.

We have shown here that a sample of 150 emerging ARs is sufficient to test the predictions of the rising flux tube model (“LNT”) with a signal-to-noise ratio about 8 at 3 days before emergence. The detection, or lack of detection of these magnetic flux concentrations, would provide important constraints on models of rising flux tubes and dynamo models in general.

We thank an anonymous referee for helpful suggestions. The work of A.C.B. was supported by NASA NNH07CD25C and NASA NNH06EA0C3. D.C.B. acknowledges support from NASA NNH07CD25C. Y.F. acknowledges support from NASA grants NNH09AK02I and NNX10AB81G to the National Center for Atmospheric Research (NCAR). NCAR is sponsored by the National Science Foundation.

APPENDIX

A 3D SPHERICAL INVERSION

The purpose of the inversion is to use a set of east–west travel-time differences to estimate the vector-valued flow field in three dimensions. The inversion is carried out in spherical geometry. We begin from the assumption that the flow \mathbf{v} can be approximated as

$$v_l(r, \theta, \phi) = \sum_{ijk} \alpha_{ijk,l} B_i^{(r)}(r) B_j^{(\theta)}(\theta) B_k^{(\phi)}(\phi), \quad (\text{A1})$$

where the index $l = r, \theta, \phi$ indicates the direction of the flow, r is the distance from the center of the Sun, θ is co-latitude, ϕ is longitude, the $\alpha_{ijk,l}$ are expansion coefficients, and the functions $B_i^{(r)}(r)$, $B_j^{(\theta)}(\theta)$, and $B_k^{(\phi)}(\phi)$ are smooth basis functions which here we have selected to be third-order B-splines (e.g., de Boor 2001). In the current work, the knots for the B-splines have been selected by hand to provide increased spatial resolution in the neighborhood of the rising flux tube (see Figure 2). One advantage of the use of B-splines is this freedom. In the examples shown here we have used (16, 16, 17) basis functions in the (r, θ, ϕ) directions; thus there are a total of 13,056 α coefficients.

The ray approximation (e.g., Kosovichev & Duvall 1997) can be used to compute the linear sensitivity functions (kernels) that relate travel-time differences to the flow field,

$$\delta\tau(\theta, \phi; \Delta) = \sum_{ijk,l} K_{ijk,l}(\theta, \phi; \Delta) \alpha_{ijk,l} + n(\theta, \phi; \Delta), \quad (\text{A2})$$

where n denotes the noise, Δ is the distance between the two quadrants of the travel-time measurement geometry, (θ, ϕ) is the location of the midpoint between the two quadrants, K are the kernel functions, and the α are the expansion coefficients of Equation (A1).

The inversion procedure consists of minimizing the function X which depends on the B-spline coefficients α as

$$X(\alpha) = \sum_{\theta, \phi, \Delta} \sigma(\theta, \phi; \Delta)^{-2} \left| \sum_{ijk,l} K_{ijk,l}(\theta, \phi; \Delta) \alpha_{ijk,l} - \delta\tau(\theta, \phi; \Delta) \right|^2 + \lambda \iiint \|v(r, \theta, \phi)\|^2 r^2 \sin\theta dr d\theta d\phi, \quad (\text{A3})$$

where λ is the regularization parameter, which controls the trade-off between matching the measurements (first term) and controlling the amplitude of the solution (second term). Here, we use the integral of the square of the solution as the regularization term; other choices are possible (e.g., demanding smoothness). As discussed in the text, Equation (A3) assumes that the noise is uncorrelated.

REFERENCES

- Braun, D. C., & Birch, A. C. 2008, [ApJ](#), **689**, L161
- Chang, H., Chou, D., & Labonte, B. The TON Team 1997, [Nature](#), **389**, 825
- Chang, H., Chou, D., & Sun, M. 1999, [ApJ](#), **526**, L53
- Couvidat, S., Gizon, L., Birch, A. C., Larsen, R. M., & Kosovichev, A. G. 2005, [ApJS](#), **158**, 217
- de Boor, C. 2001, *A Practical Guide to Splines* (New York: Springer-Verlag)
- Duvall, T. L., Jr., Jefferies, S. M., Harvey, J. W., & Pomerantz, M. A. 1993, [Nature](#), **362**, 430
- Fan, Y. 2008, [ApJ](#), **676**, 680
- Fan, Y. 2009, *Living Rev. Sol. Phys.*, **6**, 4
- Gizon, L., & Birch, A. C. 2004, [ApJ](#), **614**, 472
- Gizon, L., & Birch, A. C. 2005, *Living Rev. Sol. Phys.*, **2**, 6
- Hill, F. 1988, [ApJ](#), **333**, 996
- Jensen, J. M., Duvall, T. L., Jr., Jacobsen, B. H., & Christensen-Dalsgaard, J. 2001, [ApJ](#), **553**, L193
- Jouve, L., & Brun, A. S. 2009, [ApJ](#), **701**, 1300
- Komm, R., Howe, R., & Hill, F. 2009, [Sol. Phys.](#), **258**, 13
- Kosovichev, A. G. 1996, [ApJ](#), **461**, L55
- Kosovichev, A. G. 2009, [Space Sci. Rev.](#), **144**, 175
- Kosovichev, A. G., & Duvall, T. L., Jr. 1997, in *SCORE'96: Solar Convection and Oscillations and their Relationship*, ed. F. P. Pijpers, J. Christensen-Dalsgaard, & C. S. Rosenthal (*Astrophysics and Space Science Library*, Vol. 225; Dordrecht: Kluwer), 241
- Kosovichev, A. G., Duvall, T. L., Jr., & Scherrer, P. H. 2000, [Sol. Phys.](#), **192**, 159
- Kosovichev, A. G., & Stenflo, J. O. 2008, [ApJ](#), **688**, L115
- Nordlund, Å., Stein, R. F., & Asplund, M. 2009, *Living Rev. Sol. Phys.*, **6**, 2
- Scherrer, P. H., et al. 1995, [Sol. Phys.](#), **162**, 129
- Zharkov, S., & Thompson, M. J. 2008, [Sol. Phys.](#), **251**, 369